# An Advanced High Energy-Efficiency Rechargeable Aluminum-Selenium Battery

Shiqi Liu<sup>a</sup>, Xu Zhang<sup>a</sup>, Shiman He<sup>a</sup>, Yushu Tang<sup>c</sup>, Jie Wang<sup>a</sup>, Boya Wang<sup>a</sup>, Shu Zhao<sup>a</sup>,
Heng Su<sup>a,d</sup>, Yang Ren<sup>e</sup>, Liqiang Zhang<sup>b,c,\*</sup>, Jianyu Huang<sup>b</sup>, Haijun Yu<sup>a,\*</sup>, and Khalil Amine<sup>d,\*</sup>

<sup>a</sup> College of Materials Science and Engineering, Key Laboratory of Advanced Functional Materials, Education Ministry of China, Beijing University of Technology, Beijing 100124, P. R. China. E-mail: <u>hj-yu@bjut.edu.cn</u>

<sup>b</sup> Clean Nano Energy Center, State Key Laboratory of Metastable Materials Science and Technology, Yanshan University, Qinhuangdao 066004, P. R. China. E-mail: <a href="mailto:liqiangzhang85@163.com">liqiangzhang85@163.com</a>

<sup>c</sup> State Key Laboratory of Heavy Oil Processing, Department of Materials Science and Engineering, China University of Petroleum, Beijing Changping 102249, P. R. China.

<sup>d</sup> Chemical Sciences and Engineering Division, Argonne National Laboratory, 9700 South Cass Avenue, Lemont, IL 60439, USA. E-mail: <a href="mailto:amine@anl.gov">amine@anl.gov</a>

<sup>e</sup> X-ray Science Division, Advanced Photon Source, Argonne National Laboratory, 9700 South Cass Avenue, Lemont, Argonne, IL, USA.

#### **Abstract**

Aluminum-ion batteries (AIBs) are considered as a promising alternative to traditional rechargeable batteries due to their high theoretical capacity, low cost, and multivalent-ion/multi-electron transfer, but are hindered from commercialization by the lack of suitable cathode materials. Herein, an aluminum-selenium (Al-Se) battery that operates at room temperature with high energy efficiency is reported. This Al-Se battery exhibits high selenium utilization with a discharge capacity of 607 mAh g<sup>-1</sup>, a reduced overpotential, and high volumetric capacity for over 100 cycles. Furthermore, *ex-situ* spectroscopic and microscopic investigations of the Se cathodes indicated the existence of an aluminum selenide component as the discharge product. Additionally, *in-situ* transmission electron microscopy provided not only insights into understanding the Al-Se electrochemistry, but also a real-time characterization technique to evaluate the electrochemistry of AIBs in general.

# **Highlights**

A new aluminum-selenium (Al-Se) battery is demonstrated.

The results show a high energy-efficiency Se cathode in aluminum-ion batteries.

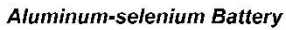
The reaction mechanism of multielectron/multivalent-ion transfer is proposed.

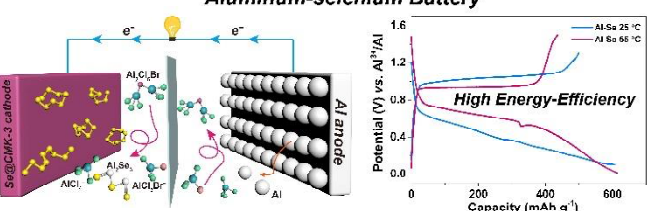
*In-situ* TEM test was first performed on the multivalent-ion battery systems.

# **Keywords**

Aluminum-ion battery, aluminum-selenium battery, high energy efficiency, reaction mechanism, in-situ TEM

# Graphical abstract





# 1. Introduction

Remarkably, lithium-ion batteries have remained the power system of choice for electronic devices, smart grids, and electric vehicles since their first commercialization by Sony Corporation around three decades ago.[1-3] The main advanced secondary batteries under development are based on monovalent cations (Li<sup>+</sup>, Na<sup>+</sup>, and K<sup>+</sup>). Attaining high energy density in these configurations is still retarded by the limited number of electrons transferred, making the monovalent rechargeable batteries far from satisfactory. Recently, state-of-the-art multivalent cation batteries (Mg, Zn, Ca, and Al metal) have shown promise due to their environmentally benign, reliable, and cost-effective characteristics, as well as their excellent electrochemical behavior.[4-7]

Of the multivalent systems, non-aqueous rechargeable aluminum-ion batteries (AIBs) have drawn considerable attention because aluminum can deliver three electrons during the charge/discharge process, resulting in fourfold higher volumetric capacity (8046 mAh cm<sup>-3</sup>) compared to lithium (2062 mAh cm<sup>-3</sup>). They also exceed other multi-electron reaction systems with respect to gravimetric capacity.[7-9] A series of AIB studies has been conducted with a variety of nanomaterials, including determination of the conversion mechanisms of sulfides and chlorides and the intercalation mechanisms of oxides, halogens, and many carbon-based materials.[10-16] Several crucial challenges impede commercialization of multivalent systems, such as poor cathode performance and limited suitable electrolytes.[17, 18] Recent reports suggest that the rechargeable aluminum-sulfur (Al-S) system is one of the most promising multi-electron-transfer batteries because of its high energy density.[19-21] Yet up to now, Al-S test batteries have suffered from limited cycle life and rapid capacity fade because of the essential features of sulfur, namely, its low electronic and ionic conductivity, the insolubility of the S<sup>2-</sup> and S<sup>-</sup> reaction product, and the shuttle effect of the polysulfides.

Selenium, because of its comparable chemical properties to sulfur, has been introduced into the family of secondary batteries. [22] More importantly, selenium offers approximately more than 20 orders of magnitude higher electronic conductivity  $(1.0 \times 10^{-3} \text{ S cm}^{-3} \text{ vs. } 0.5 \times 10^{-27} \text{ S cm}^{-3})$ 

than that of sulfur, yielding higher active materials utilization to realize rapid electrochemical reactions and better rate performance.[23, 24] Although the theoretical gravimetric capacity of selenium (675 mAh g<sup>-1</sup>) is inferior to that of sulfur, it possesses a comparably high volumetric capacity density of 3247 mAh cm<sup>-3</sup> on account of its higher density (4.81 g cm<sup>-1</sup> at 25 °C). This high volumetric capacity density can realize the use of Al-Se devices in limited spaces. Se systems also offer a higher output voltage than that of S, which can provide higher energy densities, the key performance factor for next-generation applications. Furthermore, previous reports suggest that the shuttle effect is probably more limited in the Se chemistry.[22, 25] In addition, the energy efficiency problems are ascribed to the serious overpotential loss of discharge and charge (>700 mV in Al-S systems).[19, 20] The electrode materials would suffer severe chemo-mechanical destruction during the repeated phase changes or electrochemical alloying/dealloying processes under huge polarization, leading to a seriously limited cycle stability. However, the higher electric conductivity of Se attributes to a reduced overpotential, showing a promise to acquire a high energy efficiency in Al-Se systems. Given the above considerations, Al-Se systems are a promising battery prospect-- on a par with Al-S systems.

Up to now, there has been no report of Se<sup>0</sup> reduction in a reaction with aluminum ion. We here introduce Al-Se electrochemistry on the basis of two-electron transfer during Se<sup>0</sup> reduction to Se<sup>2-</sup> with performance close to the theoretical capacity. Herein, we also propose a high-energy-efficiency Al-Se battery system. The underlying mechanisms of the Al-Se chemistry were investigated with *ex-situ* characterizations, including X-ray diffraction (XRD), Raman spectroscopy, X-ray photoelectron spectroscopy (XPS), and transmission electron microscopy (TEM). We found that the presence of AlSe<sub>x</sub> species, including Al<sub>2</sub>Se<sub>3</sub>, as electrochemical discharge products, realize the reduction of Se<sup>0</sup>. We conducted *in-situ* TEM analysis of the Al-Se system to observe, for the first time, real-time electrochemical reactions in a multivalent-ion battery. Both the spectroscopic and microscopic measurements provide valid proofs to identify the products of the conversion process and pave the way to complete understanding of the reaction mechanism.

# 2. EXPERIMENTAL

## 2.1 Preparation of Se@CMK-3 Cathode

Selenium (Aladdin) and CMK-3 carbon (XFNANO) were used without any further purifications and treatments. Se@CMK-3 was mixed with selenium powder and CMK-3 in 1:1 weight ratio and sealed in a quartz tube with Ar atmosphere. Then, the mixture was calcined at 260 °C for 12 h and 600 °C for 3 h to obtain the Se@CMK-3 composite.

#### 2.2 Materials Characterization

The total mass of selenium in the composite was 45 wt%, substantiated by thermogravimetric analysis (TG) with a SHIMADZU DTG-60H thermo balance in  $N_2$  atmosphere with 10 °C min<sup>-1</sup> heating rate from 28 °C to 800 °C (TG test shown in Fig. S1). X-ray diffraction (XRD) patterns were measured by a Bruker D8 advance equipment (Cu K $\alpha$ 1 radiation,  $\lambda$ =1.5406 Å). X-ray photoelectron spectroscopy (XPS) was conducted with a PHI Quantera II instrument to test the chemical valence state of different states of the samples. Raman characterization was carried out on a Renishaw instrument with a 532 nm laser. Field-emission scanning electron microscopy (SEM), transmission electron microscopy (TEM), and *in-situ* TEM were conducted with FEI QUANTA 650, TITAN G2 60-300, and FEI Tecnai F20 instruments, respectively.

#### 2.3 Fabrication of Al-Se Battery

The cathodes of Al-Se battery are consisted of 80 wt% Se@CMK-3, 10 wt% polytetrafluoroethylene (PTFE) binder, and 10 wt% Super P carbon. The electrode films were cut into disk with the diameter of 6 mm and pressed onto molybdenum (Mo) meshes.[26] Then the electrodes were dried at 70 °C for 20 h in a vacuum oven. Ionic liquid (IL) electrolytes were prepared with aluminum chloride and 1-ethyl-3-methyl-imidazolium bromide (Shanghai Cheng Jie Chemical Co. LTD) in 1.3 mole ratio. A piece of aluminum foil and Whatman GF/D film were served as the anode and separator, respectively. The Al-Se batteries were assembled by a customized Swagelok configuration in an argon glovebox.

#### 2.4 Electrochemical Characterization

The cycle performance was determined on a LAND battery testing system, where 1 C equals 675 mA  $\rm g^{-1}$  and 1675 mA  $\rm g^{-1}$  based on the mass of Se and S, respectively. Cyclic voltammetry testing was conducted on a Solartron electrochemical workstation at the scan rate of 0.1 mV  $\rm s^{-1}$ .

## 2.5 In-situ nanobattery setup

To prepare the Se nanowire cathode for *in-situ* TEM testing, Se powder was covered on a carbon nanotube@anodic aluminum oxide template, then the mixture was heated at 350 °C for 12 h. After cooling to room temperature, the templates were immersed in hydrofluoric acid for 24 h to obtain the Se nanowire cathode. The nanobattery was constructed through a two-probe configuration in a TEM (FEI, F20, and 200 kV). The Se nanowires were glued to an aluminum rod with conductive epoxy. Pure metal aluminum rod was used as the reference and counter electrode. A drop of EMIBr/AlCl<sub>3</sub> IL was coated on the surface of the metal Al used as an IL electrolyte for ion transportation. Both the Se nanowire and Al electrodes were mounted onto a TEM-STM (scanning tunneling microscopy) holder (Pico Femto FE-F20 holder) inside a glove box. Then, the holder was sealed in a home-built air-tight bag filled with dry argon and transferred to the TEM. The total time of exposure to the air was less than 2 s in order to avoid solidification of EMIBr/AlCl<sub>3</sub> IL electrolyte.

#### 2.6 Computational method

All theoretical calculations were performed with density functional theory (DFT), as implemented in the Vienna *ab initio* simulation package (VASP).[27, 28] The electron exchange and correlation energy was treated within the generalized gradient approximation in the Perdew-Burke-Ernzerhof functional (GGA-PBE).[29] The spin-polarized Kohn-Sham equations were expanded in a plane-wave basis set defined by a kinetic energy cut-off of 400 eV, whereas the Brillouin zone was sampled at the  $\Gamma$ -point. The convergence criteria for the electronic self-consistent iteration and force were set to  $10^{-5}$  eV and 0.02 eV/Å, respectively.

# 3. Results and Discussion

The cathode was fabricated by the encapsulation of selenium into a CMK-3 mesoporous carbon matrix after heating at 260 °C, leading to a uniformly distributed Se@CMK-3 composite (Fig. S2). The high quality of the Se@CMK-3 cathode was first evaluated in Li-Se batteries, which delivered a high capacity of 375 mAh  $g^{-1}$ , with similar charge/discharge profiles to those reported for Li-Se batteries (Fig. S3), revealing the successful fabrication of the Se@CMK-3 cathode. Then, we assembled Al-Se batteries using the Se@CMK-3 cathode, a piece of Al foil as anode, and 1-ethyl-3-methyl-imidazolium bromide/AlCl<sub>3</sub> ionic liquid (EMIBr/AlCl<sub>3</sub> IL) as electrolyte in a Swagelok configuration (Fig. 1a). Ideally, multi-electron transfer takes place in the electrochemistry of the Al-Se battery, following a total reaction of 2Al + 3Se  $\leftrightarrow$  Al<sub>2</sub>Se<sub>3</sub>, to provide a theoretical capacity of 675 mAh  $g^{-1}$  (3247 mAh cm<sup>-3</sup>). In Li-Se batteries, the formation of polyselenides did not appear during the discharging process; instead, Se<sup>0</sup> transformed to Se<sup>2</sup>-directly.[23, 25] We speculate that Al<sub>2</sub>Se<sub>3</sub> can be similarly formed in the electrochemical reaction of Al-Se systems, and thus the Al-Se batteries operate by the reversible reduction/oxidation of Se/Al<sub>2</sub>Se<sub>3</sub>.

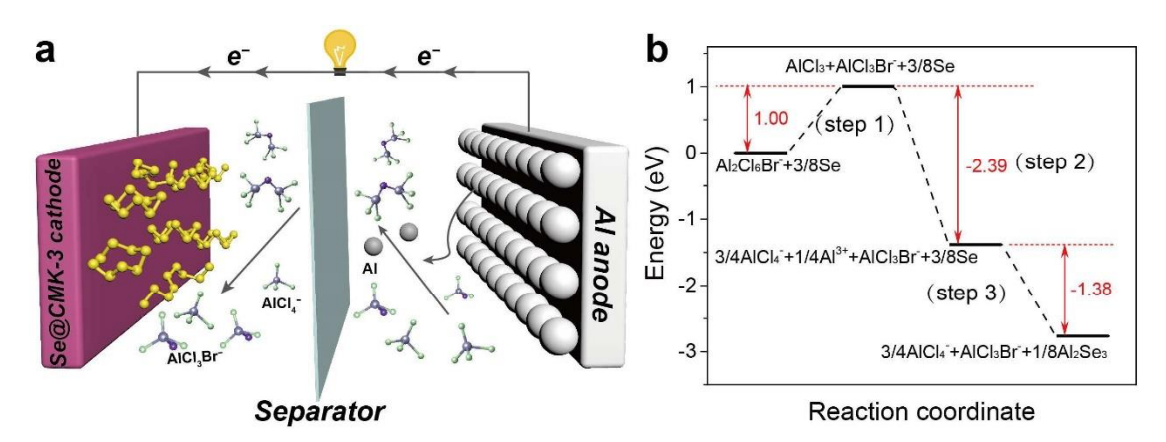


**Fig. 1. Schematic Illustration of Al-Se Battery Configuration and Its Electrochemical Reaction Energy Diagram.** (a) Schematic diagram of the rechargeable Al-Se battery assembled with a Se@CMK-3 cathode, EMIBr/AlCl<sub>3</sub> IL electrolyte, and an Al foil anode. (b) Energy plots of the dissociation and association of reactants for the operation of Al-Se battery.

On the basis of these results, the following equations are proposed for the electrochemistry of Al-Se batteries:

Discharge process:

Cathode:  $3Se + 8Al_2Cl_6Br^- + 6e^- \rightarrow Al_2Se_3 + 8AlCl_3Br^- + 6AlCl_4^- (1)$ 

Anode:  $2Al + 8AlCl_3Br^- + 6AlCl_4^- - 6e^- \rightarrow 8Al_2Cl_6Br^-$  (2) Charge process:

Cathode:  $Al_2Se_3 + 8AlCl_3Br^- + 6AlCl_4 - 6e^- \rightarrow 3Se + 8Al_2Cl_6Br^-$  (3)

Anode:  $8Al_2Cl_6Br^- + 6e^- \rightarrow 2Al$   $8AlCl_3Br^- + 6AlCl_4$  (4)

Overall:  $2Al + 3Se \rightleftharpoons Al_2Se_3(5)$ 

Based on Eq. 1, the dissociation and association energies of related reactants in this Al-Se battery have been examined by first-principle calculations, and the energy plots are shown in Fig. 1b. The first transformation is related to the dissociation of Al<sub>2</sub>Cl<sub>6</sub>Br<sup>-</sup> into intermediate AlCl<sub>3</sub> and AlCl<sub>3</sub>Br<sup>-</sup> (step 1), which further generates active Al<sup>3+</sup> cations (step 2) to electrochemically react with Se to form Al<sub>2</sub>Se<sub>3</sub> (step 3). The activation energy (step 1) for this overall reaction is 1.00 eV, and the following two steps (step 2 and 3) are exothermic processes delivering energies of -2.39 eV and -1.38 eV, respectively. The relatively lower activation energy for this overall reaction than the dissociation of Al<sub>2</sub>Cl<sub>7</sub><sup>-</sup> guarantees the efficient and fast reaction between Al and Se in this Al-Se battery (Fig. S4).[30]

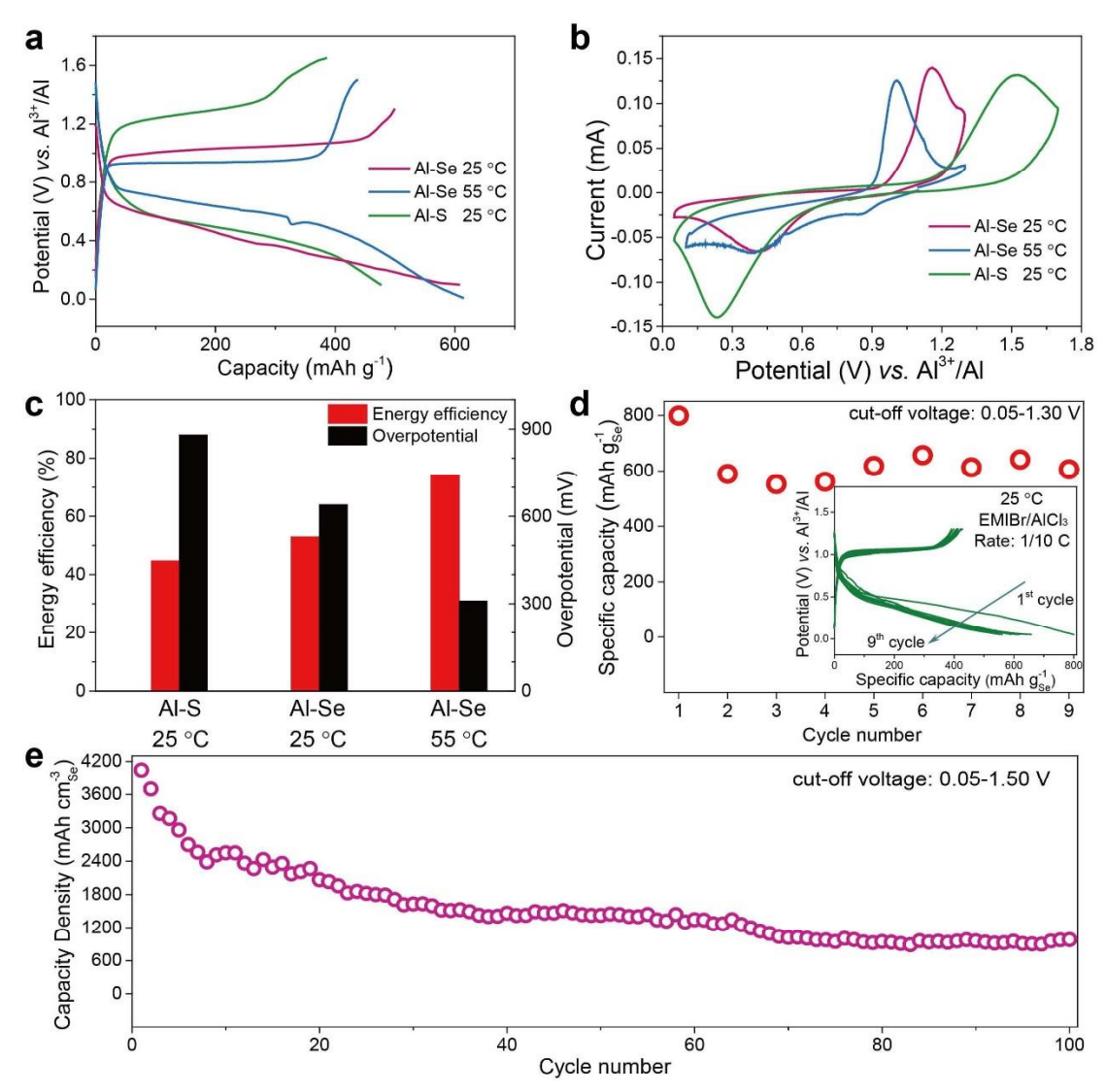


**Fig. 2. Electrochemical Performance of the Al-Se Battery.** (a) Typical charge/discharge curves of Al-Se batteries operated at 25 °C and 55 °C and Al-S batteries operated at 25 °C. (b) Cyclic voltammetry curves of the Al-Se and Al-S batteries in (a) recorded at a scan rate of 0.1 mV s<sup>-1</sup>. (c) Histogram of energy efficiencies and overpotentials of the three batteries in (a). (d) Cycle stability of Al-Se battery with cut-off voltage of 0.05-1.30 V at 25 °C. The inset shows the galvanostatic discharge/charge curves of the battery at a rate of 1/10 C. (e) Reversible capability density and long-cycle performance of Al-Se battery at 1/10 C and 25 °C with cut-off voltage of 0.05-1.50 V.

The performance of the as-prepared Al-Se batteries was tested at a rate of 1/10 C at 25 °C and 55 °C, and an Al-S battery was examined for comparison (1 C=675 mA g<sup>-1</sup> for Al-Se battery). The Al-S battery was similarly fabricated, with only S@CMK-3 instead of Se@CMK-3 used as cathode (1 C=1675 mA g<sup>-1</sup> for Al-S battery). Fig. 2a shows the typical discharge/charge curves

of the Al-Se and Al-S batteries. A large voltage hysteresis of around 880 mV between the charge and discharge plateaus is observed for the Al-S battery.[19, 20] In contrast, the Al-Se battery exhibits a lower voltage hysteresis of around 640 mV at 25 °C. When the temperature was elevated to 55 °C, the voltage hysteresis of the Al-Se battery further decreased to 310 mV. The voltage hysteresis can be sharply suppressed due to the faster kinetics of the battery operated at elevated temperature. However, the charge plateau of the Al-S battery is significantly larger than that of Al-Se battery, by around 200 mV, at the same temperature of 25 °C. This finding suggests that the kinetics, roundtrip efficiency, and cycle stability of the Al-Se battery are higher than those of the Al-S battery owing to the higher conductivity of Se.[19, 20]

The typical cycle curves of the above three batteries are in agreement with their cyclic voltammetry profiles in Fig. 2b, in which the different overpotentials can also be clearly observed. As a result, the energy efficiencies (the ratio of discharge specific energy density to the charge specific energy density) of the Al-S battery at 25 °C and the Al-Se batteries at 25 °C and 55 °C are 44%, 53%, and 74%, respectively (Fig. 2c). Therefore, higher energy efficiency represents higher reversibility of the Se cathode in the Al-Se battery, thus a better cycle stability.[31] Moreover, the Al-Se battery delivers a discharge capacity of ~600 mAh g<sup>-1</sup> for 9 cycles (Fig. 2d), corresponding to a very high Se utilization of 90%. On the contrary, the Al-S battery only delivers a discharge capacity of 476 mAh g<sup>-1</sup>, corresponding to a very poor S utilization of 28% (electrochemical performance at 55 °C is shown in supporting information Fig. S5). The electrochemical impedance spectroscopy results (Fig. S6) show a lower resistance of the Al-Se battery than that of the Al-S battery, giving another reason for the higher energy efficiency of the former system.

As evident in Fig. 2d, the Se@CMK-3 cathode exhibits an initial discharge capacity of more than 800 mAh g<sup>-1</sup>, which is over the theoretical value, a phenomenon also observed in Li-Se and Na-Se batteries. This finding implies that the extra capacity arises from the carbon host (Fig. S7) and the formation of a solid electrolyte-interface film.[23, 32-34] The cycling capability of the Se@CMK-3 cathode was further investigated in Fig. 2e. At the voltage range of 0.05-1.50 V, the

capacity density of the cathode can reach ~2200 mAh cm<sup>-3</sup> (the theoretical capacity density of Al-Se battery is 3247 mAh cm<sup>-3</sup>) for the initial 20 cycles at 1/10 C. Even after 100 cycles, a high capacity density of >980 mAh cm<sup>-3</sup> can be maintained. Thus, both the Al anode and Se cathode contribute to the high volumetric capacity of this advanced electrochemical system. In addition, the bare CMK-3 electrode only contributes a very low capacity (Figs. S7 and S8), suggesting the capacity contribution of the carbon host is ignorable. In all, the Al-Se battery proves to be a promising high-energy-density battery for limited-space applications.

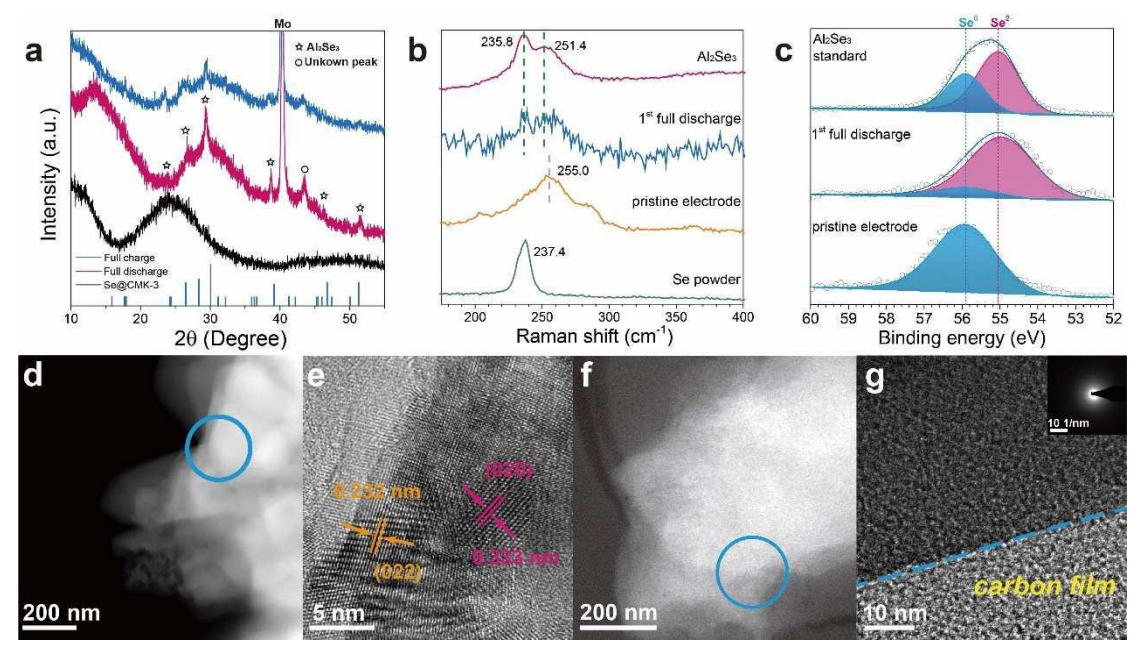


**Fig. 3.** *Ex-situ* **Spectroscopic and Microscopic Characterizations of the Se Cathodes.** (a) XRD patterns of Se@CMK-3 cathodes before battery operation, after the 1<sup>st</sup> full discharge, and after the 1<sup>st</sup> full charge. (b) Raman spectra of Al<sub>2</sub>Se<sub>3</sub> powder, Se@CMK-3 cathode after the 1<sup>st</sup> full discharge, pristine cathode, and Se powder. (c) XPS Se 3d spectra of Al<sub>2</sub>Se<sub>3</sub> powder, Se@CMK-3 cathode after the 1<sup>st</sup> full discharge, and pristine cathode. (d-g) *Ex-situ* TEM studies of Se@CMK-3 cathodes after the 1<sup>st</sup> full discharge (d, e) and after the 1<sup>st</sup> full charge (f, g).

To elucidate the electrochemistry of the Al-Se battery, we conducted *ex-situ* spectroscopic and microscopic characterizations, including XRD, Raman, XPS, and TEM, to identify the electrode components and structures at different charge/discharge stages. XRD is sensitive to the overall crystalline structures and their changes during charge/discharge of the tested electrodes. As can be seen in Fig. 3A, the pristine Se@CMK-3 cathode shows no Se peaks, suggesting the excellent dispersion of nanosized Se into the mesopores of CMK-3.[23, 34] After the 1<sup>st</sup> full

discharge, characteristic XRD peaks for Al<sub>2</sub>Se<sub>3</sub> appeared, confirming the proposed reaction route in Eqs. 1 and 2. Further charge of the cathode led to the significant fading of the Al<sub>2</sub>Se<sub>3</sub> peaks, indicating the reverse reaction of Al<sub>2</sub>Se<sub>3</sub> into amorphous Se. The trace peaks of Al<sub>2</sub>Se<sub>3</sub> after charge likely originated from the isolated or inactive Al<sub>2</sub>Se<sub>3</sub> particles in the cathode, which is disadvantageous to the efficiency of the cathode. Raman spectra with a 532 nm laser were further used to examine the structural transformation of the cathodes. The spectrum of pristine Se@CMK-3 cathode (Fig. 3B) shows that the characteristic peak of Se at 237 cm<sup>-1</sup> had shifted to 256 cm<sup>-1</sup>, indicating that the first-order A<sub>1</sub> symmetric bond stretching modes of trigonal crystalline Se converted into Se single helix and Se<sub>8</sub> molecules due to the accommodation of Se permeated into CMK-3.[35, 36] After the initial full discharge, two Raman peaks appeared at 251.4 and 235.8 cm<sup>-1</sup>, which agree well with the peaks obtained from commercial Al<sub>2</sub>Se<sub>3</sub> powders. In addition, ex-situ XPS was carried out to measure the valence change of the Se cathode (XPS survey spectra are shown in Fig. S9). After tentatively fitting the spectra, the binding energy of the Se 3d peak was found to decrease from 55.9 eV to 55.1 eV after the full discharge, indicating the conversion of Se<sup>0</sup> to Se<sup>2-</sup> in this process. Overall, the XRD, Raman, and XPS studies demonstrate that the transformation of the Se cathode into Al<sub>2</sub>Se<sub>3</sub> takes place when the Al-Se battery is discharged, confirming the proposed reaction routes of Eqs. 1 to 5.

To further examine the evolution of the cathode during the discharge/charge processes, *exsitu* TEM was applied to analyze the local structures. A scanning transmission electron microscopy image with high-angle annular dark field (HAADF) and energy dispersive X-ray spectroscopy (EDX) maps of the 1<sup>st</sup> full discharged products are displayed in Figs. 3d and S10. The latter shows a uniform distribution of Al signal in the Se region. The Al<sub>2</sub>Se<sub>3</sub> nanocrystallites that formed were further investigated by high-resolution TEM (HRTEM), as shown in Fig. 3e. The Al<sub>2</sub>Se<sub>3</sub> (022) and (020) planes are clearly observed from the HRTEM image, which provides concrete evidence for the formation of Al<sub>2</sub>Se<sub>3</sub>. Moreover, the further full charge of the cathode led to the formation of amorphous Se, as evidenced by the HAADF image, selected area electron diffraction (SAED) pattern, and the EDX maps (Figs. 3f, 3g, and S11, respectively).

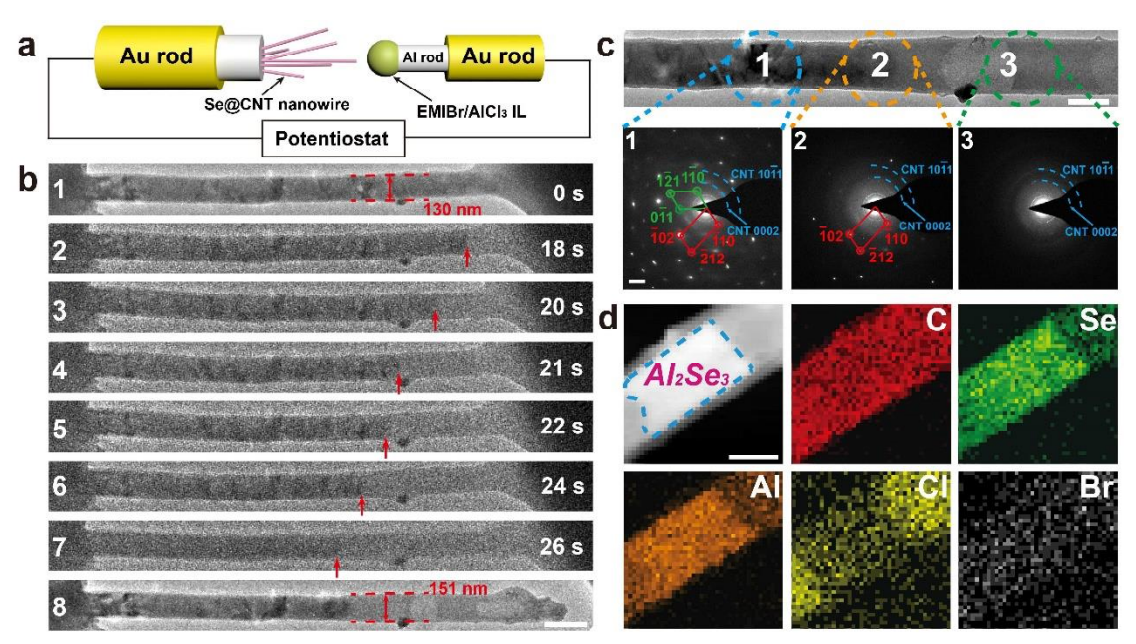


**Fig. 4.** *In-Situ* **TEM Tests of An Al-Se nanobattery.** (a) Schematic illustration of the *in-situ* Al-Se nanobattery. (b) Evolution of the Se nanowire cathode in the *in-situ* Al-Se nanobattery, after operating for different time (scale bar: 200 nm). (c) SAED patterns recorded at different positions of a partially reacted Se nanowire (scale bar: 2 1/nm). The calibrated electron diffraction patterns (EDPs) with green and red numbers are belonging to the zone axis of Se [111] and Se [221], respectively. (d) HAADF image and EDX elemental maps of a typical reacted area of Se nanowire (scale bar: 100 nm).

*In-situ* TEM studies can provide high-resolution and real-time information on the microstructural evolution of electrodes.[37, 38] However, there is a great challenge to fabricate Al-ion nanobatteries in the TEM, as the traditional liquid electrolytes are quite sensitive to air/H<sub>2</sub>O, and they can quickly solidify even before being inserted into the TEM chamber. To solve this problem, we introduced the relatively stable EMIBr/AlCl<sub>3</sub> IL electrolyte and assembled a novel Al-Se nanobattery in the TEM for characterizing its changes during electrochemical reaction. In this nanobattery system, a selenium nanowire sealed in a carbon nanotube (CNT) served as the cathode, EMIBr/AlCl<sub>3</sub> IL as the electrolyte, and an aluminum rod as the anode (Fig. 4a). The detailed method for assembling the battery can be found in the experimental procedures.

As shown in Fig. 4b-1, the pristine Se@CNT nanowire was straight with a darker contrast in the core (Se nanowire) and brighter outside (CNT). After contact with the EMIBr/AlCl<sub>3</sub> IL electrolyte, due to the surface tension of the IL, it forms an obvious meniscus on the contracting point between the nanowire and IL electrolyte. To accelerate the electrochemical reaction, a potential of –0.7 V was then applied to the nanowire with respect to the Al counter electrode. It is found that the initial activation of this Al-Se nanobattery requires no more than 18 s, and then

a clear reaction front is propagated along the longitudinal direction of the nanowire away from the IL electrolyte (Fig. 4b-8, and Movie S1). As the reaction front propagated, the diameter of the nanowire increased from 130 nm to 151 nm, and the TEM image contrast changed from typical crystalline diffraction contrast to a gray contrast characteristic of an amorphous phase. Furthermore, the phase conversion speed is relatively uniform and fast, at around 30 nm/s along the nanowire.

From a close inspection of the reaction front (Fig. 4c), we found that a volume expansion is happening in the reaction front during the first discharge. The volume expansion of this Se nanowire cathode is ~35%, slightly lower than the theoretical volume expansion (calculated as 40% by the volume change from Se to Al<sub>2</sub>Se<sub>3</sub>), which is due to the physical restriction by the CNT. Immediately after Al<sup>3+</sup> cations were generated from the Al<sub>2</sub>Cl<sub>6</sub>Br<sup>-</sup> anions, the pristine crystal Se nanowire quickly transformed into Al<sub>2</sub>Se<sub>3</sub> nanocrystals dispersed in an amorphous matrix (Fig. 4c-1 and 2). Since the IL electrolyte is inserted into the CNT as the reaction proceeds, the Al<sub>2</sub>Se<sub>3</sub> nanocrystals are dispersed in the IL electrolyte. After prolonged reaction, the EDPs of the Se nanowire totally transformed from sharp points into amorphous haloes (Fig. 4c-3).

To better characterize the reaction product, we extracted the nanowire sample from the EMIBr/AlCl<sub>3</sub> IL after reaction for a short period. As the nanowire is away from the IL electrolyte, a portion of the liquid recirculates, and an obvious reaction product appears in the nanotubes (Figs. 4d and S12). The elemental distributions in the EDX maps provide direct evidence that the main discharge product of the Al-Se nanobattery is AlSe<sub>x</sub> species, which agrees well with the theoretical calculation and *ex-situ* experimental results. In addition, we found that the IL electrolyte can diffuse across the produced Al<sub>2</sub>Se<sub>3</sub> nanoparticle into the CNT, which helps the fast and continuous reaction between Se and Al<sup>3+</sup> in this nanobattery.

In summary, we established the high-energy-efficiency, room-temperature, rechargeable Al-Se battery at the macro-, micro-, and nanoscale. Our Al-Se battery with ionic liquid electrolyte possesses high Se cathode utilization, a good reversible capacity of 607 mAh g<sup>-1</sup>, a reduced overpotential of 640 mV, long-term cycle capability for over 100 cycles, and high volumetric capacity in both Al and Se electrodes suitable for use in limited spaces. The results of our electrochemical thermal analyses show a high energy efficiency of 53% and 74% at 25 °C and 55 °C, respectively. Moreover, spectroscopic and microscopic analyses of the cathode revealed

the details of the electrochemical behavior for the discharge product Al<sub>2</sub>Se<sub>3</sub> in the Al-Se system. *In-situ* TEM results of the Al-Se nanobattery showed a direct view of the reaction process and discharge products. This Al-Se chemistry has great potential in the development of secondary multivalent and multi-electron-transfer batteries.

#### **ACKNOWLEDGEMENTS**

We appreciate the financial supports from the National Natural Science Foundation of China (Grants 51622202, 21603009, and 21875007), the National Key R&D Program of China (Grant No. 2018YFB0104302), Beijing Natural Science Foundation (B) (KZ201910005002), and Beijing Natural Science Foundation of China-Haidian Special Project (L182065). This research used resources of the Advanced Photon Source, a U.S. Department of Energy (DOE) Office of Science User Facility operated for the DOE Office of Science by Argonne National Laboratory under Contract No. DE-AC02-06CH11357. We thank Dr. Cheng-Jun Sun for his valuable comments.

#### **AUTHOR CONTRIBUTIONS**

H.Y., K.A., and L.Z. conceived and designed the project. S.L. synthesized the Se@CMK-3 sample and performed the electrochemical tests. S.L., X.Z., S.H., J.W., H.S., Y.R., and K.A. performed spectroscopic characterizations and analyzed the data. Y.T., L.Z., and J.H. conducted the *in-situ* TEM tests. B.W. performed *ex-situ* TEM tests. S.Z. performed the DFT calculations. S.L., X.Z., L.Z., H.Y., and K.A. wrote and polished the manuscript. All authors analyzed the data and contributed to the discussion.

#### DECLARATION OF INTERESTS

The authors declare no competing interests.

# REFERENCES

- [1] M. Armand, J.M. Tarascon, Nature, 451 (2008) 652.
- [2] J.M. Tarascon, M. Armand, Nature, 414 (2001) 359-367.
- [3] H. Yu, H. Zhou, J. Phys. Chem. Lett., 4 (2013) 1268-1280.
- [4] J.W. Choi, D. Aurbach, Nat. Rev. Mater., 1 (2016) 16013.

- [5] F. Wang, O. Borodin, T. Gao, X. Fan, W. Sun, F. Han, A. Faraone, J.A. Dura, K. Xu, C. Wang, Nat. Mater., 17 (2018) 543-549.
- [6] D. Wang, X. Gao, Y. Chen, L. Jin, C. Kuss, P.G. Bruce, Nat. Mater., 17 (2017) 16. [7] Y. Zhang, S. Liu, Y. Ji, J. Ma, H. Yu, Adv. Mater., 30 (2018) 1706310.
- [8] Y. Hu, D. Ye, B. Luo, H. Hu, X. Zhu, S. Wang, L. Li, S. Peng, L. Wang, Adv. Mater., 30 (2018) 1703824.
- [9] M. Walter, K.V. Kravchyk, C. Böfer, R. Widmer, M.V. Kovalenko, Adv. Mater., 30 (2018) 1705644.
- [10] T. Koketsu, J. Ma, B.J. Morgan, M. Body, C. Legein, W. Dachraoui, M. Giannini, A. Demortière, M. Salanne, F. Dardoize, H. Groult, O.J. Borkiewicz, K.W. Chapman, P. Strasser, D. Dambournet, Nat. Mater., 16 (2017) 1142.
- [11] S. Gu, H. Wang, C. Wu, Y. Bai, H. Li, F. Wu, Energy Storage Mater., 6 (2017) 9-17.
- [12] H. Tian, S. Zhang, Z. Meng, W. He, W.-Q. Han, ACS Energy Lett., 2 (2017) 1170-1176.
- [13] M.-C. Lin, M. Gong, B. Lu, Y. Wu, D.-Y. Wang, M. Guan, M. Angell, C. Chen, J. Yang, B.-J. Hwang, H. Dai, Nature, 520 (2015) 324.
- [14] H. Chen, H. Xu, S. Wang, T. Huang, J. Xi, S. Cai, F. Guo, Z. Xu, W. Gao, C. Gao, Sci. Adv., 3 (2017) eaao7233.
- [15] J. Wang, X. Zhang, W. Chu, S. Liu, H. Yu, Chem. Commun., 55 (2019) 2138-2141.
- [16] S. Jiao, H. Lei, J. Tu, J. Zhu, J. Wang, X. Mao, Carbon, 109 (2016) 276-281.
- [17] F. Wu, H. Yang, Y. Bai, C. Wu, Adv. Mater., 31 (2019) 1806510.
- [18] H. Yang, H. Li, J. Li, Z. Sun, K. He, H.-M. Cheng, F. Li, Angew. Chem., Int. Ed., 131 (2019) 2-23.
- [19] T. Gao, X. Li, X. Wang, J. Hu, F. Han, X. Fan, L. Suo, A.J. Pearse, S.B. Lee, G.W. Rubloff, K.J. Gaskell, M. Noked, C. Wang, Angew. Chem., Int. Ed., 55 (2016) 9898-9901.
- [20] W. Chu, X. Zhang, J. Wang, S. Zhao, S. Liu, H. Yu, Energy Storage Mater., 22 (2019) 418-423.
- [21] X. Yu, A. Manthiram, Adv. Energy Mater., 7 (2017) 1700561.
- [22] A. Abouimrane, D. Dambournet, K.W. Chapman, P.J. Chupas, W. Weng, K. Amine, J. Am. Chem. Soc., 134 (2012) 4505-4508.
- [23] C.-P. Yang, S. Xin, Y.-X. Yin, H. Ye, J. Zhang, Y.-G. Guo, Angew. Chem., Int. Ed., 52 (2013) 8363-8367.
- [24] X. Li, J. Liang, X. Li, C. Wang, J. Luo, R. Li, X. Sun, Energy Environ. Sci., 11 (2018) 2828-2832.
- [25] Y. Cui, A. Abouimrane, C.-J. Sun, Y. Ren, K. Amine, Chem. Commun., 50 (2014) 5576-5579.
- [26] J. Shi, J. Zhang, J. Guo, ACS Energy Lett., 4 (2019) 2124-2129.
- [27] G. Kresse, J. Furthmüller, Comput. Mater. Sci., 6 (1996) 15-50.
- [28] G. Kresse, J. Furthmüller, Phys. Rev. B, 54 (1996) 11169-11186.
- [29] J.P. Perdew, K. Burke, M. Ernzerhof, Phys. Rev. Lett., 77 (1996) 3865-3868.
- [30] H. Yang, L. Yin, J. Liang, Z. Sun, Y. Wang, H. Li, K. He, L. Ma, Z. Peng, S. Qiu, C. Sun, H.-M. Cheng, F. Li, Angew. Chem., Int. Ed., 57 (2018) 1898-1902.
- [31] Z. Zhu, A. Kushima, Z. Yin, L. Qi, K. Amine, J. Lu, J. Li, Nat. Energy, 1 (2016) 16111.

- [32] J. Ding, H. Zhou, H. Zhang, T. Stephenson, Z. Li, D. Karpuzov, D. Mitlin, Energy Environ. Sci., 10 (2017) 153-165.
- [33] S.-K. Park, J.-S. Park, Y.C. Kang, ACS Appl. Mater. Interfaces, 10 (2018) 16531-16540.
- [34] H. Ye, Y.-X. Yin, S.-F. Zhang, Y.-G. Guo, J. Mater. Chem. A, 2 (2014) 13293-13298.
- [35] I.L. Li, J.P. Zhai, P. Launois, S.C. Ruan, Z.K. Tang, J. Am. Chem. Soc., 127 (2005) 16111-16119.
- [36] I.L. Li, S.C. Ruan, Z.M. Li, J.P. Zhai, Z.K. Tang, Appl. Phys. Lett., 87 (2005) 071902.
- [37] X.H. Liu, L.Q. Zhang, L. Zhong, Y. Liu, H. Zheng, J.W. Wang, J.-H. Cho, S.A. Dayeh, S.T. Picraux, J.P. Sullivan, S.X. Mao, Z.Z. Ye, J.Y. Huang, Nano Lett., 11 (2011) 2251-2258.
- [38] J.Y. Huang, L. Zhong, C.M. Wang, J.P. Sullivan, W. Xu, L.Q. Zhang, S.X. Mao, N.S. Hudak, X.H. Liu, A. Subramanian, H. Fan, L. Qi, A. Kushima, J. Li, Science, 330 (2010) 1515.